Environment International 145 (2020) 106153

Contents lists available at ScienceDirect

Environment International

journal homepage: www.elsevier.com/locate/envint

Biomass burning spatiotemporal variations over South and Southeast Asia

Shuai Yin

Center for Global Environmental Research, National Institute for Environmental Studies, Tsukuba 3058506, Japan

ARTICLE INFO

Handling Editor: Xavier Querol

Keywords:
Crop residue burning
Forest fire
Siegel's repeated median
Standard deviation ellipse
Time series

ABSTRACT

In this study, Moderate Resolution Imaging Spectroradiometer active fire and land use products were integrated to extract and classify biomass burning (BB) data for South Asia (SA) and Southeast Asia (SEA). Several trend and geographic distribution analyses were conducted at the grid (0.25° × 0.25°) and regional scales. As the principal local form of BB, crop residue burning (CRB) in SA increased by 844 spots/yr, and the Mann–Kendall (MK) τ reached 0.61. Additionally, the CRB in Punjab-Haryana, a region a well-known for severest CRB, presented a significant declining trend. BB in mainland SEA was much more intense and was dominated by forest and shrubland fires. Forest fires in mainland SEA declined at a rate of −209 spots/yr, and shrubland fire conversely grew at a rate of 803 spots/yr, which was likely related to the dramatic land cover change induced by the local swidden agriculture. Unlike other regions, BB in equatorial SEA primarily occurred in the second half of the year (August to October), and it was extremely vulnerable to El Niño events. When the annual sea surface temperature anomalies within the Niño 3 region improved by 1 °C, the annual BB spots and fire radiative power in equatorial SEA increased by 5.18×10^4 and 2.40×10^6 MW, respectively. Although the interannual variations in equatorial SEA were dramatic, the robust Siegel's repeated median estimator still revealed that equatorial SEA BB significantly declined by −1825 spots/yr. This regional decline reflects government endeavors to curb indigenous BB. However, regions with enhanced BB still need to draw more attention, and it is imperative for the Indonesian government to take substantial measures to reduce anthropogenic fire sources during El Niño events.

1. Introduction

Human-initiated biomass burning (BB) is a widespread practice for deforestation, shifting cultivation, and post-harvest vegetative material removal. It is also an important factor in shaping the landscape over a long evolutionary scale (Hao and Liu, 1994; Hayasaka et al., 2014; Itahashi et al., 2018). BB immediately releases greenhouse gases (GHGs) into the atmosphere and induces a long-term shift in the balance between ecosystem carbon sequestration and liberation (Lorenz and Lal, 2010; Konovalov et al., 2014). Climatic changes, e.g., global warming, are expected to change BB regimes, and they may accelerate the accumulation of GHGs in the atmosphere, thus leading to further global warming (Bond-Lamberty et al., 2007). Massive amounts of particulate matter emissions from BB decease atmospheric visibility, causing severe haze pollution and increasing respiratory and cardiovascular morbidity, mortality, and hospital admissions (Arbex et al., 2007, 2010; Lin et al., 2018; Marlier et al., 2013; Pun et al., 2017; Reddington et al., 2015). As the primary aerosol released from BB, carbonaceous particles contribute to variations in the global radiation budget (Myhre et al., 2013). Moreover, BB is the second-largest source of trace gases; volatile organic compounds and NO_x emitted from BB are critical precursors of global tropospheric O_3 and secondary aerosols (Bo et al., 2008; Lin et al., 2013). Many studies have found that BB is not only a local pollution source. Through long-range transport, BB pollutants pose a severe threat to the health of those living in downstream regions, and they can even induce severe pollution episodes in adjacent countries (McClure and Jaffe, 2018; Afroz et al., 2003; Koe et al., 2001). BB types range from open forest fires to biofuel burning (Akagi et al., 2011). The cause, location, and timing of each BB type are difficult to determine. Typically, crop residue burning (CRB) is closely linked to certain farming activities and crop types. In contrast, forest fires and other wildfires are assumed to be linked to both natural and anthropogenic factors such as lightning ignition and land clearing.

BB frequently occurs in most parts of South Asia (SA) and Southeast Asia (SEA). Fires in equatorial SEA are highly affected by droughts induced by the El Niño–Southern Oscillation (ENSO). Over the past four decades, three devastating forest fires have occurred in Sumatra and Borneo in 1982/1983, 1997/1998, and 2015. These ENSO-driven forest fires released massive GHGs into the atmosphere, and the most severe fire, which occurred in 1997/1998, was estimated to emit 0.95 Gt of

E-mail address: yin.shuai@nies.go.jp.

https://doi.org/10.1016/j.envint.2020.106153
Received 12 July 2020; Received in revised form 16 September 2020; Accepted 18 September 2020
Available online 12 October 2020
0160-4120/© 2020 The Author(s). Published by Elsevier Ltd. This is an open access article under the CC BY-NC-ND license (http://creativecommons.org/licenses/by-nc-nd/4.0/).

carbon (van der Werf et al., 2010; Turetsky et al., 2015). The landscape in mainland SEA is characterized by mountainous areas, and swidden agriculture is a consistent threat to indigenous forests. Most BB in mainland SEA is attributed to slash-and-burn agriculture and land clearing, especially during the dry season (Chang and Song, 2010; Shi et al., 2014). Kumar et al. (2011) revealed that springtime CRB in northern Indian can increase the levels of surface O_3 and black carbon by 34% and 145%, respectively. Furthermore, strong convections during the summer monsoon season can also transport pollutants from SA to the Mediterranean Sea (Lawrence et al., 2003; Park et al., 2007).

Because the BB characteristics in SA/SEA are inhomogeneous and cannot be monitored at the ground-level, it is essential to apply remote sensing technology to specify the spatiotemporal variations of BB. Some of the most widely used satellite data in BB studies are the Moderate Resolution Imaging Spectroradiometer (MODIS) fire products, which exhibit temporal coverage from February 2000 to present day. MODIS was designed to take measurements in a broad spectral range, and it can extend and enhance many heritage sensor observations (Xiong et al., 2015; Xiong et al., 2006). Previous BB studies over SA/SEA focused on estimating the related emissions and assessing their effects on ambient air quality (Liu et al., 1999; Lelieveld et al., 2001; Engling et al., 2011; Sahu and Sheel, 2014). In this study, we collected MODIS fire and land cover data from 2001 to 2018 to reveal the seasonal patterns and spatiotemporal variations of various BB types over SA/SEA. Additionally, we integrated active fire spot data with fire radiative power (FRP) data, an important combustion rate physical metric, to determine the fire characteristics. Analyses were conducted at several scales, including at a 0.25° × 0.25° grid-scale, instead of only at a large scale, e.g., regional- or country-scale. Furthermore, the repeated median trend, which is less sensitive to outliers, and monotonic trend combined with a directional distribution analysis were utilized to explicitly illustrate the interannual variations. Precipitation and ENSO events, which are important climate factors that affect BB, are also considered to further explore the fire–climate relationship. Given the inhomogeneity of BB and vast expanse of the study region, the results of this work can be utilized by policy makers to mitigate BB and reduce local air pollution.

2. Datasets and methodology

2.1. Datasets

2.1.1. Fire information

The MOD14A1 Collection 6 data, with a 1 km × 1 km spatial resolution, were used to obtain the fire information for SA/SEA. The MODIS Thermal Anomalies/Fire products algorithm uses brightness temperatures derived from the MODIS 4-μm and 11-μm channels. The fire detection strategy was based on the absolute detection of fires if the fires were strong enough, and detection relative to the thermal emissions of the surrounding pixels was utilized to detect weaker fires (Justice et al., 2002; Giglio et al., 2003). The improved MOD14A1 Collection 6 products reduced the global commission errors to 1.2%, compared to 2.4% for Collection 5 (Giglio et al., 2016). In this study, two fire indicators were extracted from MOD14A1: the number of daily fire spots and the corresponding FRP. A 0.25° × 0.25° grid was created to aggregate and present the BB spatial distributions over SA/SEA.

2.1.2. Land cover

MCD12Q1, which includes the land cover products, also belongs to the MODIS production series. The spatial resolution of MCD12Q1 is 500 m × 500 m, and the temporal resolution is 1 yr. Since the new millennium, rapid economic development and urbanization have induced dramatic land cover changes in SA/SEA, and numerous tropical forests in SEA have been cleared by plantation companies (Miettinen et al., 2016; Stibig et al., 2014; Fox et al., 2014). Therefore, it is vital to consider land use and land cover changes when classifying BB types. Given the high spatial resolution of MCD12Q1, it can be utilized to incorporate land use changes into this study. The primary land cover scheme of MCD12Q1 is the International Geosphere–Biosphere Program, which identified 17 land cover classes (Loveland and Belward, 1997). Combining MOD14A1 with MCD12Q1 from 2001 to 2018, BB was divided into four groups: forest fires, shrubland fires, CRB, and other fires (primarily grass and sparsely vegetated fires). Table S-1 in the supplementary material presents more information on the four groups of land cover. Additionally, we also discussed the uncertainties of MODIS fire and land cover products (refer to Section1 in the supplementary material).

2.1.3. Precipitation and SEA surface temperature

Monthly precipitation data were obtained from TerraClimate, that formed a dataset of monthly climate at a high-spatial resolution (1/24°). Abatzoglou et al. (2018) downscaled coarser resolution temporal anomalies from Climate Research Unit version 4.0 data and the Japanese 55-year Reanalysis from 1958 using high-resolution climatological fields from WorldClim and climatic aided interpolation to create TerraClimate. The data were validated using a variety of monitoring networks including the Global Historical Climate Network, Snow Telemery network, and remote automated weather stations. The results revealed that the TerraClimate dataset improved the overall mean absolute error and increased the spatial realism compared to those of the coarser resolution gridded datasets. To be consistent with the BB distribution data, the TerraClimate resolution was first aggregated to 0.25° × 0.25°, and then the spatial correlation between precipitation and BB over SA/SEA was explored. The historical SST in the four Niño regions (Niño 1 + 2, Niño 3, Niño 4, and Niño 3.4) was obtained from the National Oceanic and Atmospheric Administration (NOAA). It used Optimum Interpolation Sea Surface Temperature (OISST) v2 to calculate SST anomalies and the base period is from 1981 to 2010.

2.2. Methodology

Considering their vast range of geographic and climatic conditions, SA and SEA were divided into three subregions: SA, mainland SEA, and equatorial SEA. Fig. S-1 in the supplementary material displays the locations of the three subregions. Because the BB spatiotemporal characteristics of each subregion are distinct, a spatial analysis was also conducted at the subregional level. The seasonal patterns and interannual variations of various BB types in the three subregions were analyzed.

2.2.1. Time series trend analysis

The widely used Theil–Sen estimator was first proposed by Theil (1950), and then Sen (1968) extended this estimator to handle ties. Because it is based on the median slope, it is insensitive to outliers, and it tends to accurately calculate the slope for non-normal data (Vanem and Walker, 2013). Siegel (1982) modified the Theil–Sen estimator, replacing the single median with the repeated media, which increased the breakdown point to 50% compared to the 29% breakdown point of the original Theil–Sen estimator (Lemmens and Krag, 2014; Lavagnini et al., 2011). Siegel's repeated median estimator is calculated as follows:

$$Estimator = \underset{i}{median}\left\{\underset{j \neq i}{\text{median}}\left(\frac{x_i - x_j}{t_i - t_j}\right)\right\} \quad (1)$$

where x_i and x_j are the number of fire spots or FRP value at time t_i and t_j ($i > j$), respectively.

The Mann–Kendall (MK) statistic is a non-parametric test used to detect significant trends in a time series, and it is based on the ranks of the observations rather than their actual values (Kendall, 1955; Mann, 1945). Because the MK test is distribution-free, it has been widely used to analyze many natural time series, such as temperature, precipitation, river flow, and water quality time series (Hamed, 2009). The MK rank coefficient τ is defined as follows:

$$\tau = \frac{2}{n(n-1)} \sum_{i=1}^{n-1} \sum_{j=i+1}^{n} sgn(x_j - x_i) \quad (2)$$

where n is the number of data points, x_i and x_j are the data values in time series i and j ($j > i$), respectively, and $\mathrm{sgn}(x_j - x_i)$ is the sign function:

$$sgn(x_j - x_i) = \begin{cases} +1 if (x_j - x_i) > 0 \\ 0 if (x_j - x_i) = 0 \\ -1 if (x_j - x_i) < 0 \end{cases} \quad (3)$$

The coefficient ranges from −1 to +1 and a value of +1 represents a continuously increasing trend and never decreases. The opposite is true when τ is −1, and a value of 0 indicates no consistent trend.

2.2.2. Geographic distribution analysis

Given the inhomogeneous spatiotemporal distribution of BB, two geographic distribution analyses were used to characterize BB over SA/SEA: the standard deviation ellipse (SDE) and median center (MEC). The SDE was firstly proposed by Lefever in 1926, and ever since then, it has served as a versatile tool for bivariate distributions (Lefever, 1926; Wang et al., 2015). The SDE is a centrographic measure used to characterize the dispersion of points along two orthogonal axes. It results in an ellipse that delineates the average location, dispersion (or concentration), and orientation of all the points. The MEC is a measure of central tendency that uses an iterative algorithm to explore the location of the point that minimizes the Euclidean distance to all features in a dataset. Compared with the mean center, MEC is less sensitive to data outliers. The inter-annual variations of SDE and MEC can reveal the overall BB spatial dynamic processes over the study region. Both BB parameters were incorporated into these analyses: the number of burning spots and the corresponding FRP. To more specifically delineate the BB geographic distributions, the FRP of each BB spot was adopted as a weight factor in the geographic analysis.

3. Results and discussions

3.1. Seasonal pattern of BB

3.1.1. SA

Fig. 1 demonstrates that BB presents distinctive seasonal patterns in the three subregions. SA was dominated by CRB, which accounted for 57.30% of the annual fire spots and 39.84% of the annual FRP. Additionally, intensive CRB lasted much longer than the other BB types, and the number of burning spots exceeded 1,500 from October to the following May. The monthly CRB spots and corresponding FRP peaked at 6,043 spots and 1.71 × 10^5 MW, respectively, in May (Fig. S-2). Figs. S-3 and S-4 in the supplementary material display the box plots of monthly BB spots and FRP, respectively. According to the Indian Ministry of New and Renewable Energy, India generates 500 Mt of crop residue per year on average, nearly 100 Mt of which is burned directly on the farmland (Bhuvaneshwari et al., 2019). Fig. 2 illustrates that the most intense CRB from 2001 to 2018 was concentrated in northwestern

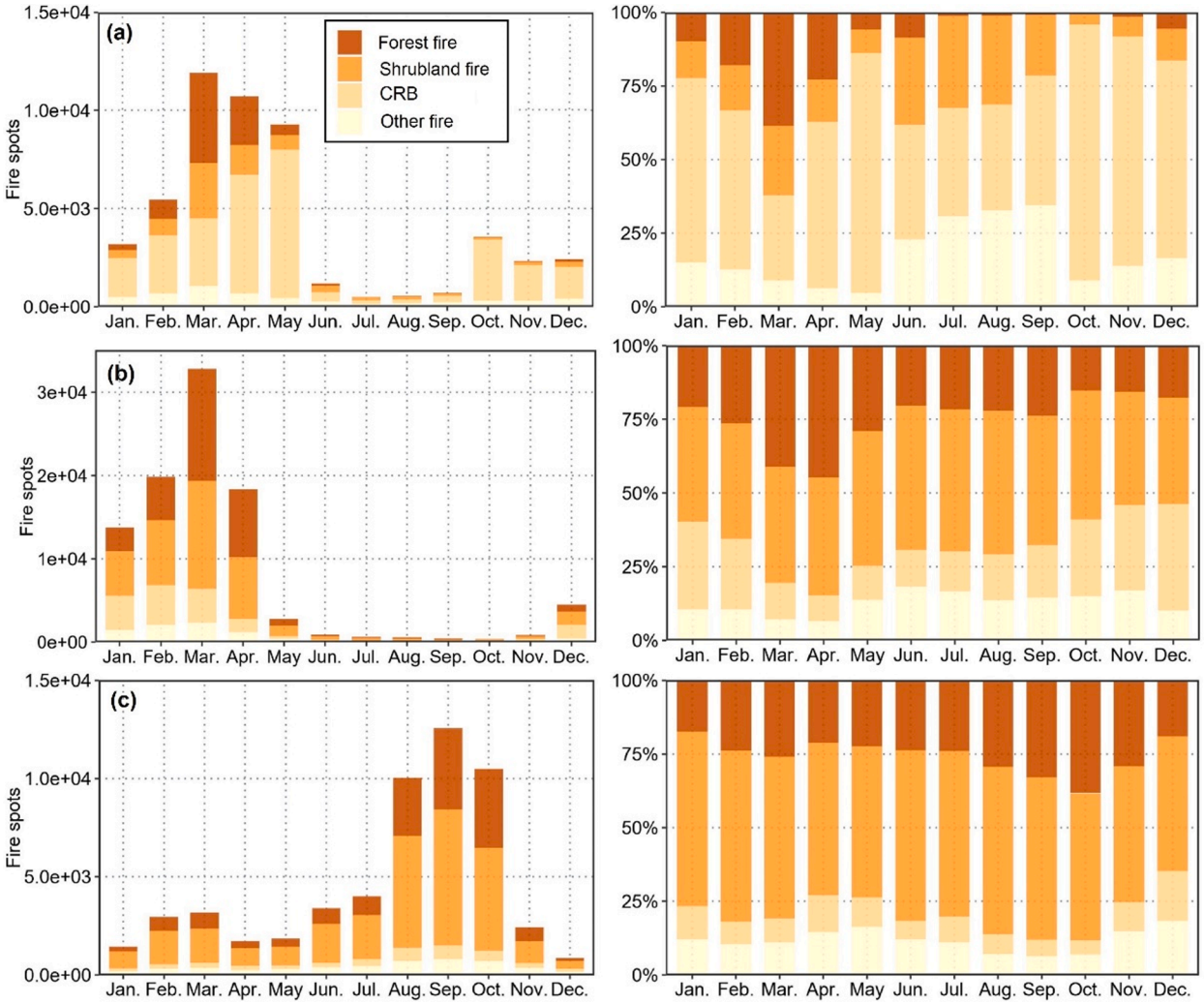

Fig. 1. Monthly BB spots over SA/SEA (left panel) and the 100% stack column chart (right panel) for (a) SA, (b) mainland SEA and (c) equatorial SEA.

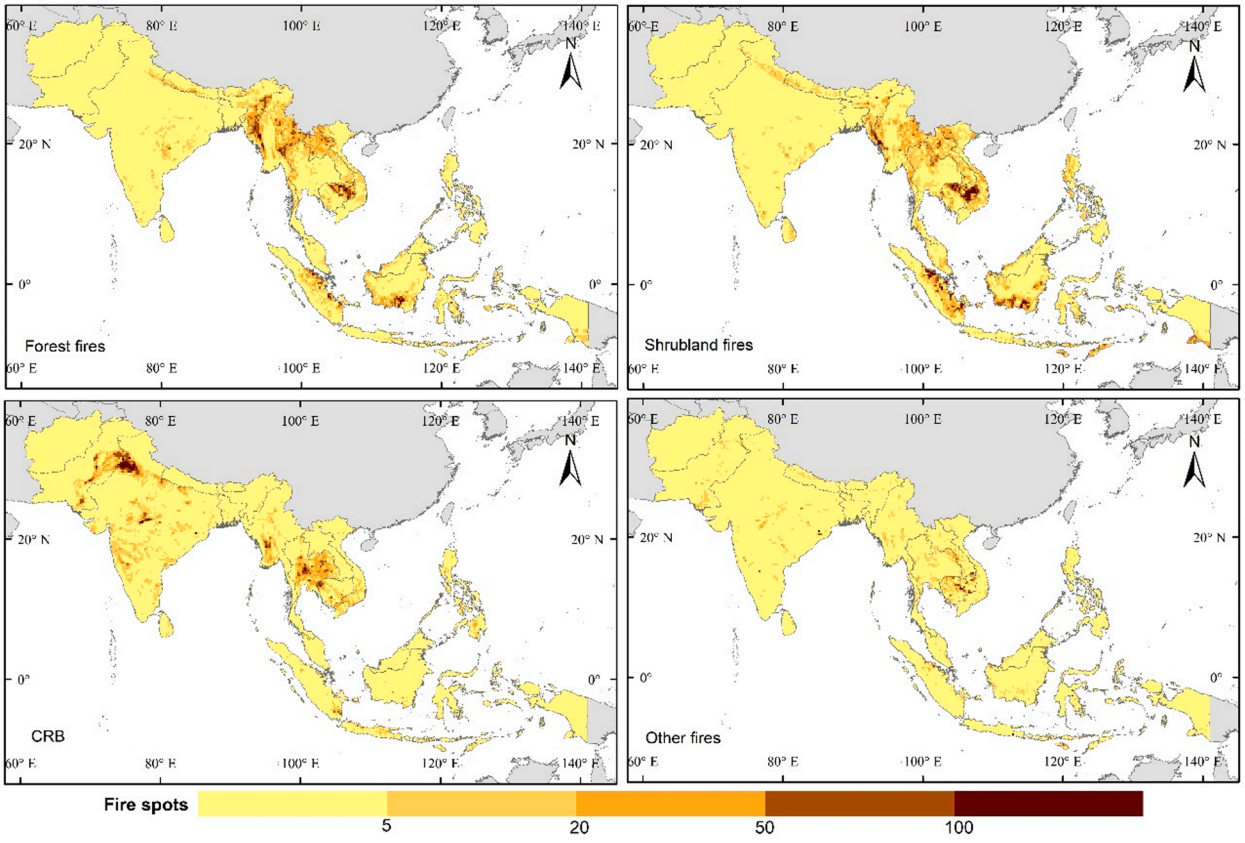

Fig. 2. Spatial distribution of annual BB spots over SA/SEA.

India, where approximately two-thirds of the national food grains are produced (Jethva et al., 2019). The principal crop system in this region was the wheat-rice crop rotation, and the subsequent harvesting left a large amount of straw in the fields (Kaskaoutis et al., 2014). With respect to the monthly spatial distribution, severe CRB first occurred in Punjab-Haryana after the rice harvesting season in October and November (Fig. S-7). Then, the CRB gradually spread to southern India (e.g., Maharashtra and Karnataka) and southeastern Pakistan (e.g., Punjab and Sindh); however, the CRB strength is much lower than that in northwestern India. Since April, the CRB in northwestern India significantly increased, coinciding with wheat harvesting, and the number of CRB spots were substantially greater than that in the previous October–November burning season. Severe CRB during April–May was also detected in central India (Madhya Pradesh), which is also an essential producer of wheat. Each year, the CRB pollutants emitted in northwestern India were transported thousands of kilometers downwind, severely deteriorating the air quality of the entire Indo-Gangetic Plain (Sharma et al., 2010). From June to September, the southwest monsoon induces abundant rainfall over India, and crops enter the important summer growing season (Auffhammer et al., 2012). Thus, Fig. 1a and Fig. S-7 indicate that there were hardly any clear CRB spots in SA during this four-month period. The second-largest BB type in SA was forest fire. Although it only constituted 17.75% of burning spots, the corresponding FRP accounted for 32.73% of the SA annual average versus 39.84% of that for CRB (Table 1). The forest fire burning season was only two months (March and April), and it peaked in March with 4592 burning spots and 3.21×10^5 MW FRP. Forest fires were primarily distributed in southern Nepal and northern India (Uttarakhand and Himachal Pradesh). Sparsely distributed forest fire spots were also found in central India (Fig. 2). The monthly variation and spatial distribution

Table 1
Summary of annual BB spots and FRP over SA/SEA.

Region		Forest fires	Shrubland fires	CRB	Other fires	Total
SA	Fire spot number	9184	7693	29,651	5223	51,751
	Fire spot percentage	17.75%	14.87%	57.30%	10.09%	100.00%
	FRP ($\times 10^5$ MW)	5.28	3.10	6.42	1.32	16.12
	FRP percentage	32.73%	19.25%	39.84%	8.18%	100.00%
	Average FRP (MW/spot)	57.4	40.3	21.7	25.2	31.1
Mainland SEA	Fire spot number	32,113	38,057	17,171	8,544	95,885
	Fire spot percentage	33.49%	39.69%	17.91%	8.91%	100.00%
	FRP ($\times 10^5$ MW)	18.14	15.78	3.84	2.75	40.51
	FRP percentage	44.77%	38.96%	9.49%	6.78%	100.00%
	Average FRP (MW/spot)	56.5	41.5	22.4	32.1	42.3
Equatorial SEA	Fire spot number	16,290	29,789	3,909	4,992	54,980
	Fire spot percentage	29.63%	54.18%	7.11%	9.08%	100.00%
	FRP ($\times 10^5$ MW)	7.16	11.58	1.01	2.13	21.87
	FRP percentage	32.72%	52.92%	4.64%	9.72%	100.00%
	Average FRP (MW/spot)	43.9	38.9	25.9	42.6	39.8

of shrubland fires is extremely similar to that of forest fires; Table 1 shows that the annual number of shrubland fire spots and FRP were 7693 and 3.10 × 10^5 MW, respectively, which were lower than those of forest fires. Other fires only constitute 10.09% of the SA burning spots, and they were sparsely distributed in central India and southern Pakistan. In March, the number of burning spots and FRP of other fires also reached peaks of 1067 and 2.76 × 10^4 MW.

3.1.2. Mainland SEA

Table 1 shows that the fire spots and FRP in mainland SEA is much higher than those in the other regions, and the annual average of FRP exceeded 4 × 10^6 MW, which is higher than that of SA and equatorial SEA combined. Additionally, the BB in this region primarily occurred from January to April, and the burning type was dominated by forest and shrubland fires (Fig. 1b), which accounted for over 70% of the annual spots and over 80% of the annual FRP. In March, the number of burning spots and FRP peaked at 32,816 and 1.65 × 10^6 MW, respectively. The forest fire spatial distribution was consistent with that of shrubland fires, and they were predominately concentrated in the northern and southeastern mainland SEA (Fig. 2). In January, the intense forest and shrubland fires only occurred in northern Cambodia. Then, the fires began to spread to northern Laos and eastern/western Myanmar in February. In March and April, the number of forest and shrubland fires in the northwestern part of mainland SEA increased dramatically, and the burning intensity was much higher than that in other regions (Figs. S-5 and S-6). We assumed that the forest and shrubland fires in the mountainous SEA were closely related to swidden agriculture. For centuries, swidden cultivation, also referred to as shifting cultivation or slash-and-burn farming, has been recognized as a rational economic choice by farmers in SEA. This practice consistently threatens indigenous forest resources and causes great amounts of deforestation (Fox et al., 2009; Mertz et al., 2009; Rerkasem et al., 2009). CRB in mainland SEA accounted for 17.91% of the annual fire spots and 9.49% of the annual FRP. Fig. 1b illustrates that the number and percentage of CRB spots started to increase in December, and the number of CRB spots and corresponding FRP peaked at 4747 and 1.07 × 10^5 MW, respectively, in February. The CRB spatial distribution was unlike those of the forest and shrubland fires. CRB was detected in Thailand in December, and it gradually increased in Thailand and the extreme west of Cambodia until March (Fig. S-7). Moreover, in February and March, intense CRB was also found in the southern part of Myanmar. Other fires only accounted for 8.91% of the annual fire spots; they were scattered in southeastern mainland SEA, and they displayed no clear aggregation from January to April (Fig. S-8).

3.1.3. Equatorial SEA

Unlike the BB of other regions, that of equatorial SEA primarily occurred during the second half of the year, especially from August to October. In September, the number of fire spots and FRP peaked at 12,568 and 4.99 × 10^5 MW, respectively (Fig. 1c and S-2c). Shrubland fire was the principal form of BB in equatorial SEA, accounting for over 50% of the annual fire spots and FRP. Fig. 2 shows that the forest and shrubland fires predominately occurred in eastern Sumatra (including Riau, Jambi, and South Sumatra) and southern Borneo (including West Kalimantan, Central Kalimantan, South Kalimantan, and North Kalimantan), where a world-renowned peatland is located. In Indonesia, peatland fires are mostly anthropogenically induced to clear land and produce ash for fertilizer (Goldammer and Seibert, 1990; Kanapathy, 1976). The growing demand for arable land, especially for oil palm plantation, has further contributed to the deforestation and drainage of peat swamp forests in Indonesia. Therefore, peatlands were more susceptible to fires during the dry season from April to October. Fig. 1 illustrates that there was hardly any intense BB in SA and mainland SEA during the wet season; the fire spot number in mainland SEA was consecutively below 1000 from July to November. In contrast, conspicuous burning was detected during the wet season in equatorial SEA. In February and March, the multi-annual average number of fire spots was nearly 3000, and this value was substantially higher in certain years, e.g., severe BB occurred in February 2014 and March 2014, and the monthly fire spot numbers reached 12,780 and 14,520, respectively, which were higher than the multi-annual average fire spots in September. The monthly spatial distribution of forest and shrubland fires demonstrated that BB in February and March only aggregated on the coastal lowland of central Sumatra (Riau Province), and hardly any BB was discovered in southern Borneo during the wet season (Figs. S-5 and S-6). CRB only constituted 7.11% of the annual burning spots, which was much lower than that in the other subregions. Fig. 2 shows that the CRB was primarily distributed in the southernmost area of Sumatra, eastern Java, and Mindanao. The number of other fires was limited in equatorial SEA, and they accounted for approximately 9% of the annual fire spots and FRP, which was slightly higher than that of CRB. Additionally, they were primarily distributed in central Sumatra and southern Borneo.

3.2. Inter-annual BB variation

Fig. 3 indicates that the number of BB spots in SA significantly increased from 2001 to 2009. In 2009, the annual fire spots and FRP were 62,300 and 1.94 × 10^5 MW, respectively. The annual values fluctuated and eventually peaked in 2012. The increasing trend in SA was primarily induced by the CRB inter-annual variation, which was the principal BB in this region. In the past 18 years, the number of CRB spots grew from 23,095 to 42,791, and the corresponding FRP nearly doubled. Fig. S-9 in the supplementary material displays the annual FRP for the study region. The forest and shrubland fires did not exhibit clear trends, and the corresponding annual number of fire spots ranged from 5000 to 15,000. In contrast, other fires showed an increasing trend, and the number of burning spots peaked at 7276 in 2016. Fig. S-10 shows that the annual fire spots aggregated along the Indo-Gangetic Plain and that BB in southern India was more dispersed, and the intensity was not as strong as that in the northern part. Unlike SA, the inter-annual variation in BB spots in mainland SEA was irregular. In 2004, 2007, and 2010, the annual number of fire spots exceeded 12,000, and the FRP exceeded 5 × 10^6 MW, which was much higher than those of the other years. Although the annual number of forest and shrubland fire spots varied stochastically in mainland SEA, the proportion of forest fires decreased from approximately 35% to 25%. In contrast, the proportion of shrubland fire spots significantly increased from approximately 35% to 42% (Fig. 3b). We assumed that this was mainly caused by the rapid land cover change in mainland SEA. Swidden agriculture has greatly contributed to indigenous deforestation, and forest area, primarily concentrated in northern Laos and Cambodia, has decreased by over 10% in the past two decades. In contrast, shrubland area had increased by approximately 15% (Yin et al., 2019). The annual number of CRB spots in this region primarily fluctuated between 12,000 and 20,000, and it peaked at 26,178 in 2005. Other fires in mainland SEA substantially increased before 2013, and the corresponding fire spots tripled to 17,340. Then, the number of other fires declined to only 6000 in 2017 and 2018. Compared with SA and equatorial SEA, Fig. S-10 shows that the fire spots in mainland SEA covered a much larger region, and the area with intense BB was further enlarged in 2004, 2007, and 2010. The inter-annual variation in equatorial SEA was the most drastic; the number of BB spots and FRP reached 145,000 and 6.58 × 10^6 MW in 2015, which was far more than those of the other years. In 2017, the BB spots in equatorial SEA declined to 14,800, which was only 10% of 2015. In addition, the coefficients of variation (CVs) of annual BB spots and FRP were 65.24% and 74.92%, respectively, in equatorial SEA. The CV in SA was only 17.31% for BB spots and 16.53% for FRP. In mainland SEA, the CVs of BB spots and FRP were 21.98% and 26.38%, respectively. In addition to 2015, there were several other peak BB years in equatorial SEA, e.g., 2002, 2006, and 2009, and the peak years likely corresponded to the warm phase of the ENSO, which is discussed in the following

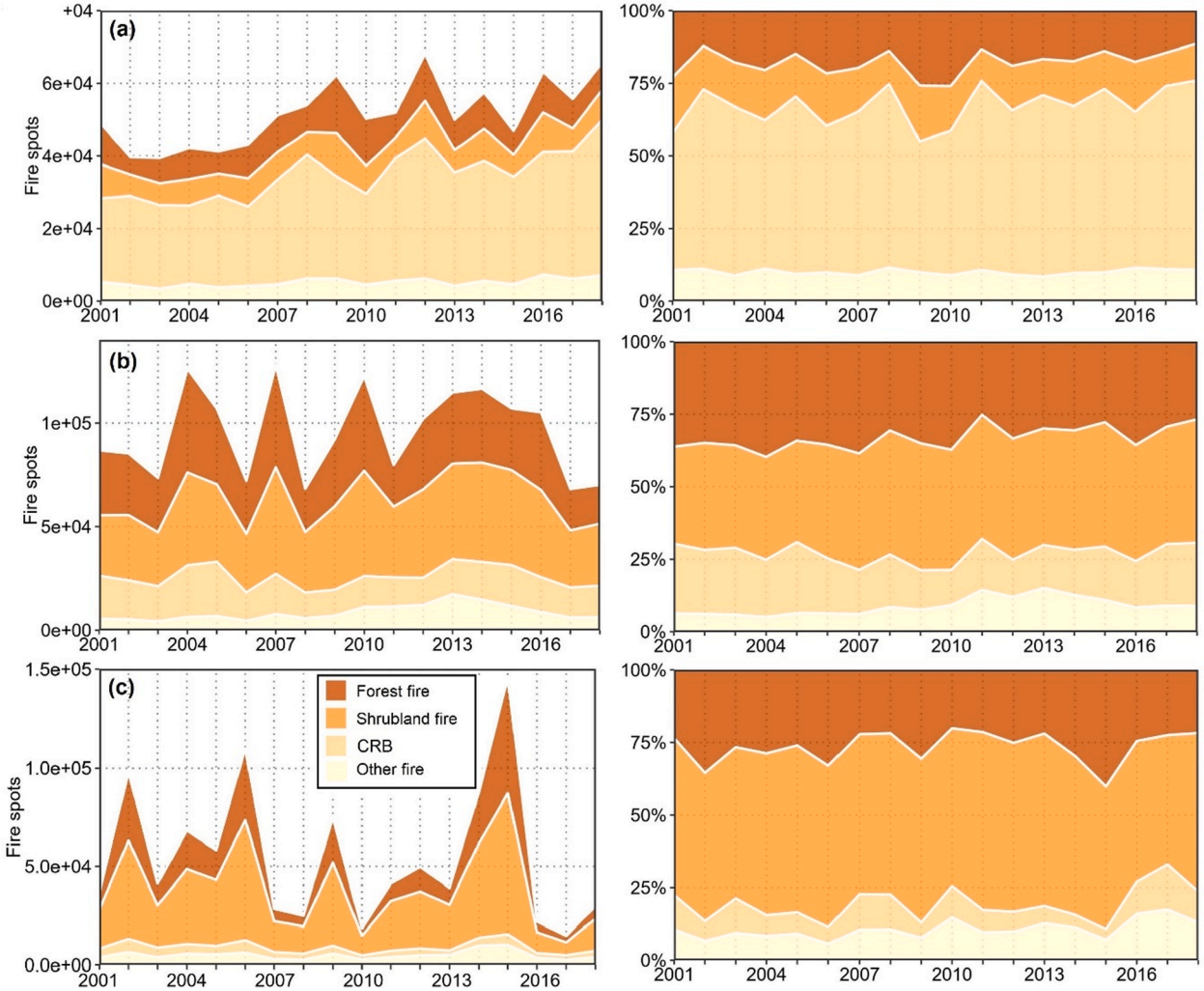

Fig. 3. Interannual variation of BB spots (left panel) and its 100% stack figure (right panel) from 2001 to 2018 for (a) SA, (b) mainland SEA and (c) equatorial SEA.

sections. Fig. 3c reveals that forest and shrubland fires greatly contributed to the increase in BB in the peak years, and the proportion of these two BB types exceeded 85% in 2002, 2006, 2009, and 2015. From 2001 to 2018, the annual BB was primarily concentrated in the Sumatra and Borneo Islands; the number of fire spots in these two islands constituted 69.70% of that of equatorial SEA. Intense BB was also detected in Indonesian New Guinea when a devastating fire occurred in 2015.

Table 2
Trend analysis of BB spot from 2001 to 2018.

Region	Trend type	Statistics parameter	Forest fire	Shrubland fire	CRB	Other fire	All BB
SA		estimator (RME)	92	55	844***	136***	1389***
	Siegel's repeated median	95% CI upper limit	160	118	1049	186	1595
		95% CI lower limit	−70	−9	792	89	1057
		τ	0.05	0.22	0.61***	0.39 *	0.54 **
	Mann-Kendall	95% CI upper limit	0.42	0.57	0.82	0.68	0.81
		95% CI lower limit	−0.32	−0.14	0.40	0.09	0.28
Mainland SEA		estimator (RME)	−209	803*	−122	480***	103
	Siegel's repeated median	95% CI upper limit	173	1043	8	655	1087
		95% CI lower limit	−852	25	−313	351	−800
		τ	−0.18	0.16	−0.18	0.44*	−0.06
	Mann-Kendall	95% CI upper limit	0.21	0.53	0.13	0.74	0.29
		95% CI lower limit	−0.57	−0.20	−0.49	0.13	−0.40
Equatorial SEA		estimator (RME)	−411*	−1083*	−172***	−33	−1825*
	Siegel's repeated median	95% CI upper limit	−95	−138	−121	91	−317
		95% CI lower limit	−1109	−1904	−212	−107	−3224
		τ	−0.2	−0.16	−0.44*	−0.07	−0.18
	Mann-Kendall	95% CI upper limit	0.16	0.21	−0.14	0.31	0.19
		95% CI lower limit	−0.57	−0.47	−0.73	−0.45	−0.55

Note: * indicates $p < 0.05$; ** indicates $p < 0.01$ and *** indicates $p < 0.001$; CI stands for confidence interval.

3.3. Trend and geographic distribution analysis

3.3.1. Time series trend analysis

BB in SA significantly increased at a rate of 1389 spots/yr, and the corresponding MK τ was 0.54 from 2001 to 2018. This is primarily induced by the variation in CRB which is the principal local BB form. Table 2 shows that the two trend indicators of CRB spots, repeated median estimator (RME) and MK τ, reached 844 spots/yr and 0.61, respectively, in SA which were much higher than those of the other BB types, and the increasing areas were mainly located in central/southern India and eastern Pakistan. Furthermore, the indicators in Madhya Pradesh (India) and Punjab (Pakistan) were even larger; the RME and MK τ exceeded 10 spots/yr per grid and 0.75, respectively (Figs. 4 and 5). In contrast, the CRB in northwestern India significantly declined, particularly in Punjab-Haryana. Considering the entire SA, the area of Punjab-Haryana is very small; however, this region accounted for approximately one third of CRB spots in SA, and the burning intensity was much stronger than that in other regions. To combat air pollution in Delhi, the Indian government has taken many measures to curb CRB in the Indo-Gangetic Plain, such as rewarding farmers who refrain from CRB and promoting the usage of alternative sustainable management methods. We infer that these measures have effectively mitigated CRB in northwestern India, while the substantially enhanced CRB in other SA regions requires more attention regarding developing sustainable management methods and improving SA ambient air quality. For the forest and shrubland fires, the burning spots presented an insignificant increasing trend in SA ($p > 0.05$), and they were primarily distributed in the Indo-Gangetic Plain and east India. While, the FRP results indicated a declining trend, where the RME was −15,217 MW/yr ($p < 0.01$) for forest fires and −3314 MW/yr ($p < 0.01$) for shrubland fires (Table S-2). Thus, we assume that although the number of forest and shrubland fire spots grew slightly in SA, the radiant heat output from these fires was significantly reduced. Analogous to CRB, the number of other fire spots also demonstrated a significant increasing trend, and the RME and MK τ were 136 spots/yr and 0.39, respectively. The increase regions of other fires were scattered in central/southern India and eastern Pakistan.

The RME of BB spots in mainland SEA was only 103 spots/yr, which was not as drastic as that of the other two regions. Indeed, the BB trend in mainland SEA was much more complex and inhomogeneous. Table 2 shows that the RME of forest fires was −209 spots/yr, and the MK τ was −0.18. This significant declining trend largely aggregated in western/eastern Myanmar and northern Cambodia, corresponding to the area with severe forest fires from 2001 to 2018 (Figs. 4 and 5). Additionally, forest fires in central Vietnam were significantly enhanced. In contrast, shrubland fires grew at a rate of 803 spots/yr, and the increase was mainly distributed in the eastern part of mainland SEA, particularly in northern Cambodia. Additionally, Figs. 4 and 5 reveal that the shrubland fire decline in western Myanmar was more drastic than that in the other regions. CRB in mainland SEA presented a decreasing trend; the burning spot and FRP RMEs were −122 spots/yr and −6381 MW/yr, respectively. The spatial distribution of CRB trend was highly random, and the regions showing the increases and decreases were blended in northeastern Thailand and southern Cambodia. For other fires, the two indicators revealed a significant increasing trend in mainland SEA that was primarily dispersed in Laos and Cambodia.

Although the previous section illustrates that the amplitude of the annual BB in equatorial SEA was much larger, there were still significant declining fire spot and FRP RME trends of −1825 spots/yr and −98,419 MW/yr, respectively. Because the shrubland fires accounted for over 50% of BB spots and FRP, its decrease rate was −1083 spots/yr, which was much higher than that of the other BB types. The decrease region of the shrubland fire was primarily distributed in southern Sumatra and Borneo, where massive peatlands were more susceptible to fire. While, the shrubland fires on the coastal lowland of central Sumatra presented

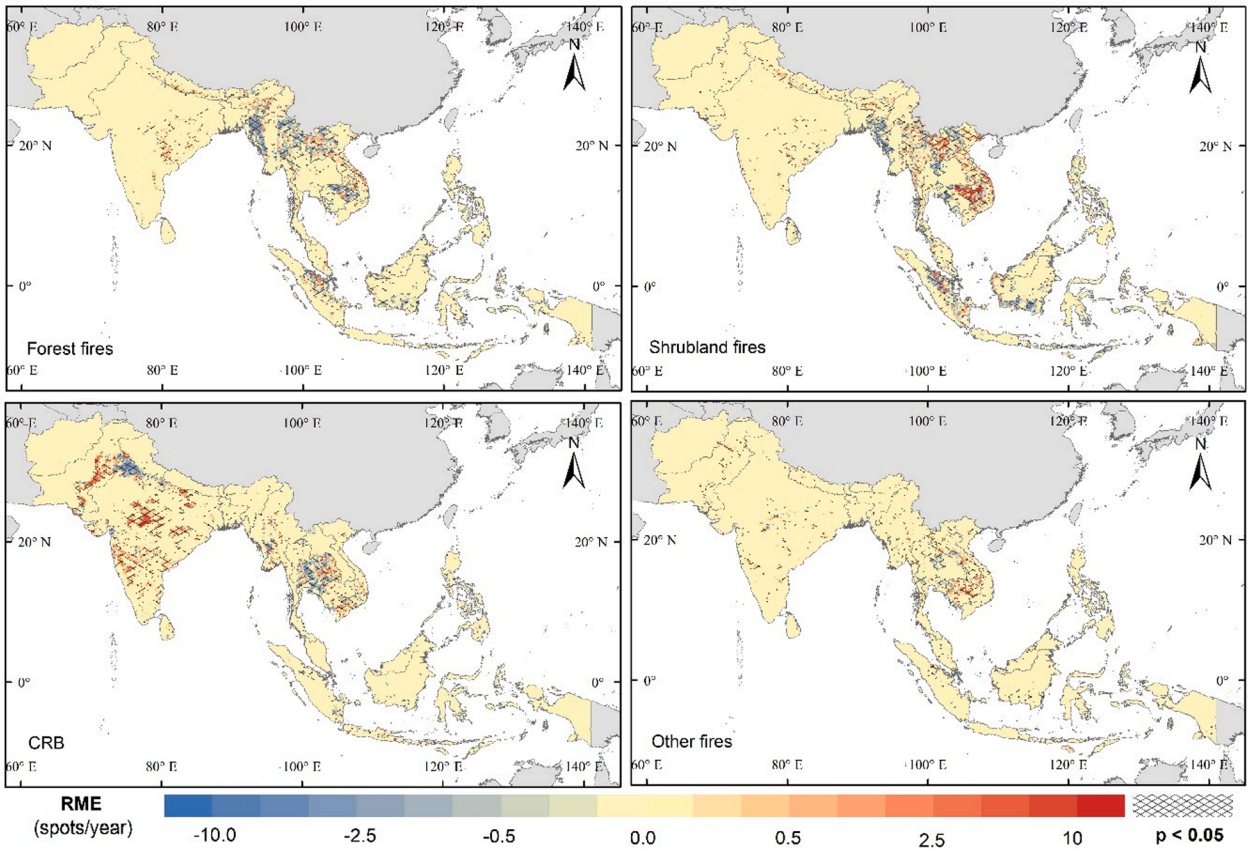

Fig. 4. Siegel's RME of BB from 2001 to 2018: the mesh indicates the significant area where $p < 0.05$.

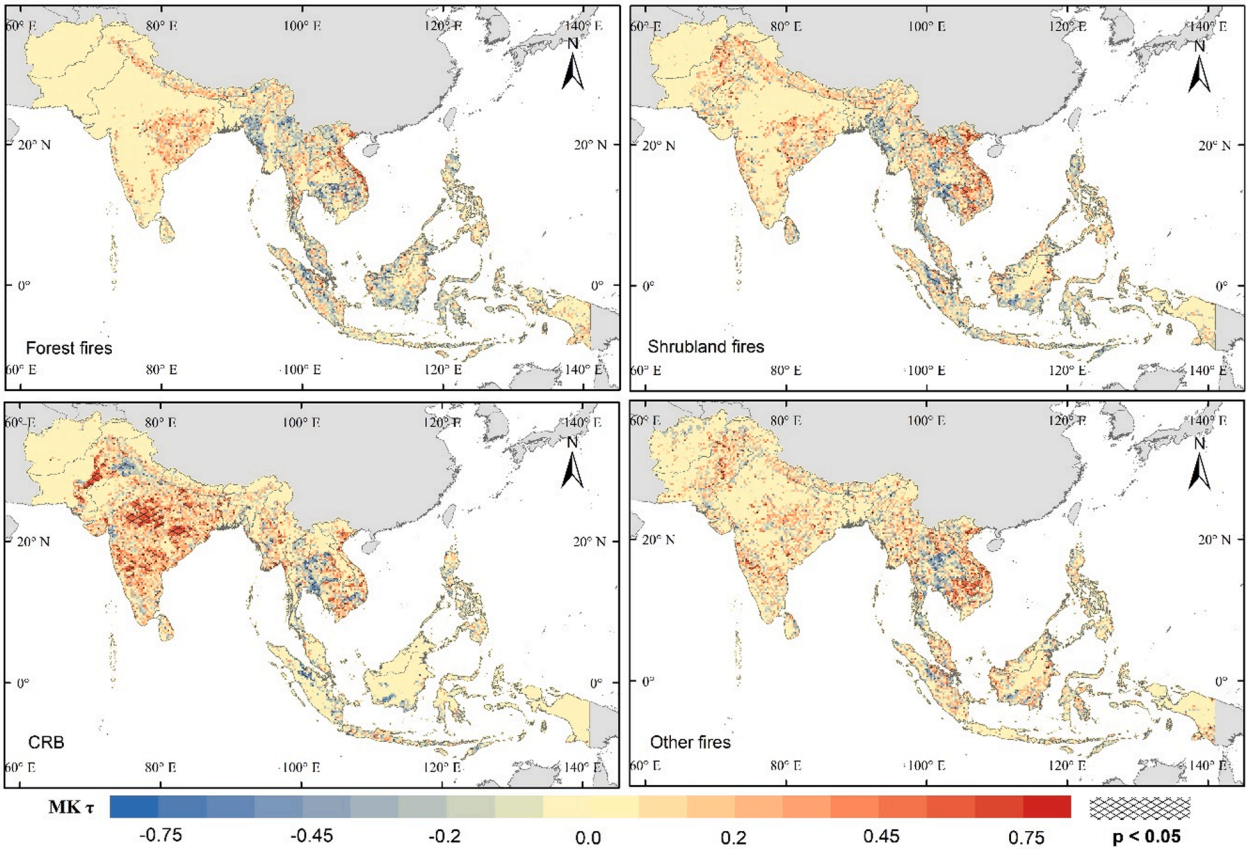

Fig. 5. Mann-Kendall τ of BB from 2001 to 2018: the mesh indicates the significant area where $p < 0.05$.

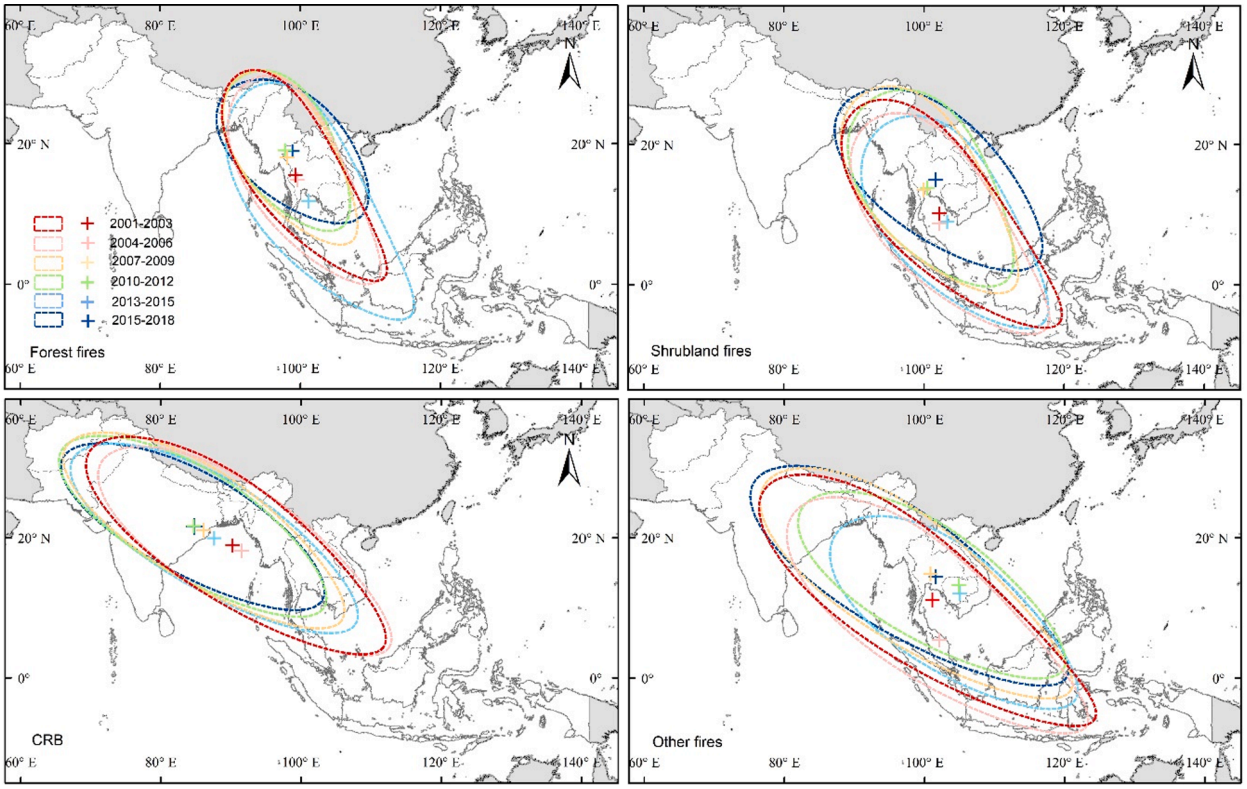

Fig. 6. Spatial variations of MEC and SDE from 2001 to 2018.

an increasing trend, and the RME of certain grids exceeded 10 spots/yr. The characteristics of the forest fire trends were consistent with those of the shrubland trends; only the RMEs were considerably lower, which were −411 spots/yr and −25,327 MW/yr for fires spots and FRP, respectively. Both trend indicators revealed that the number of CRB spots substantially decreased from 2001 to 2018; the RME and MK τ were −172 spots/yr and −0.44, respectively. The decrease region was scattered in the eastern Java, southernmost Sumatra, and southern Borneo. Other fires presented an insignificant decreasing trend, and the spatial distribution was highly dispersive and nearly negligible. Since 2000, five El Niño events have occurred, with the strongest one occurring in 2014–2016. The warm phase of the ENSO always accompanied abnormal BB in Indonesia, which could interrupt the accuracy of trend analysis. The linear trend and Theil–Sen estimator were also calculated, and the results demonstrated that they were unable to detect any significant trends in equatorial SEA. As the RME can resist up to 50% of outliers, it is more likely to disclose significant trends of this region. The results further prove that RME is a more reliable and suitable indicator for this study, rather than the linear trend or Theil–Sen estimator.

3.3.2. Geographic distribution analysis

The data time period of 18 years was divided evenly into 6 sub-periods to conduct the geographic distribution analysis. Because the distribution of forest fires was more aggregated and concentrated, its SDEs were much smaller than those of the other burning types. Fig. 6 demonstrates that the MEC of the forest fires was located in central Thailand in the first and second sub-periods (2001–2003 and 2004–2006). The enhanced forest fires in Myanmar resulted in the MEC moving northwestward, and the major axis of the SDEs also decreased in the following sub-periods. Table S-3 in the supplementary material contains the SDE and MEC features. With the devastating BB in Indonesia in 2015, the MEC moved substantially toward Sumatra and Borneo. The SDE axes also abnormally expanded to 5153 km and 1457 km, which were the longest of the six sub-periods. In the final sub-period (2016–2018), the forest fire SDEs returned to the northwest of mainland SEA, and the major axis also shrank to only 3669 km. The SDEs of the shrubland fires look extremely similar to those of the forest fires, with slightly larger sizes. The MECs of the shrubland fires were located more southeastern, and they also substantially moved toward Indonesia in the fifth sub-period (2015–2018). Because there was intense CRB in both SA and mainland SEA, the CRB SDE major axis was longer than that of the forest and shrubland fires. With the CRB intensification in India, the CRB MEC gradually moved northwestward after the second sub-period. When abnormal BB occurred in Indonesia, the CRB MEC also moved toward Sumatra and Borneo; however, this move was not as significant as that of the forest and shrubland fires. Then, the MEC returned to eastern India, and the two SDE axes were also reduced to only 5497 km and 1264 km, which were the shortest of the six sub-periods. The SDEs and MECs of other fire varied more stochastically and irregularly. The SDEs covered the entirety of SA/SEA, and the MECs were concentrated around Thailand and Cambodia. Unlike the forest fires, shrubland fires, and CRB, we did not observe the SDEs and MECs of other fires deforming and moving toward any specific direction from 2001 to 2018 (see Fig. 6).

3.4. Discussion

3.4.1. Effect of precipitation and El Niño

The correlation between monthly precipitation and BB spots was explored, and the results indicated that monthly precipitation was an important factor in constraining BB in SA/SEA (Fig. 7). The negative slopes in South Sumatra and Borneo, which were susceptible to peatland fires, were always less than −0.2 spots/mm, which was lower than that for the other regions. A negative slope was also found in northwestern India, northern Laos, eastern/western Myanmar, and central Thailand. BB in mainland SEA, especially in the southern part (e.g., Thailand and Cambodia), demonstrates stronger correlations with rainfall, and the correlation coefficient (r) reached −0.50 in most parts of southern mainland SEA (Fig. 7). Compared with the other regions, Fig. 1b shows there was hardly any BB in mainland SEA during the wet season which was possibly related to the stronger correlation with rainfall. Although the negative slopes in southern Sumatra and Borneo were greater than those in the other regions, the r only ranged from −0.25 to −0.35, which was not as significant as that of southern mainland SEA. During the wet season in equatorial SEA, intense BB still occasionally occurred in February and March; hence, a lower r was likely in this region. For SA, the correlation in the west coastal region was more significant than that in northwestern India where the BB was the severest, and the slope was approximately −0.1 spots/mm.

Because the BB of equatorial SEA was enhanced during El Niño years, it is essential to examine the correlation between the two BB indicators (number of fire spots and FRP) and SST anomalies in the four Niño regions. Fig. 8 demonstrates that in the second half of the year, the SST variation along the equatorial Pacific Ocean, especially in the Niño 3 and Niño 3.4 regions, significantly affected BB intensity in equatorial SEA, and the r was always above 0.70 ($p < 0.001$). For the BB in the first half of the year, Fig. S-11 shows that the r was always below 0.3, and it did not significantly correlate to the variation in SST anomalies along the equatorial Pacific Ocean ($p > 0.05$). When the annual SST anomalies in the Niño 3 region improved by 1 °C, the annual BB spots and FRP increased by 5.18×10^4 and 2.40×10^6 MW in equatorial SEA (Fig. S-12). To investigate whether El Niño events impacted BB in SA and mainland SEA and quantify its effect on BB intensity, a correlation analysis for annual BB and SST anomalies in the Niño 3 region was also conducted at the grid-scale. Fig. 9 indicated that the SST anomalies in the Niño 3 region tremendously affected BB in southern Sumatra and Borneo. The slope in some parts of Central Kalimantan, South Sumatra, and Jambi exceeded 200 spots/°C and 15,000 MW/°C per grid. SST anomalies in the Niño 3 region also exhibited a positive effect on BB intensity in northern Cambodia; however, it was insignificant ($p > 0.05$), and the region was limited. In contrast, BB in western Myanmar

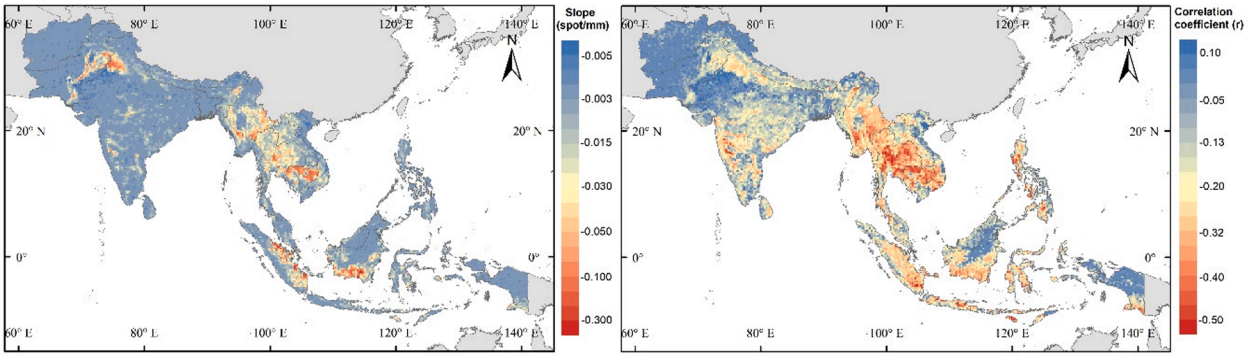

Fig. 7. Correlation between monthly precipitation and BB spot: slope (left panel); correlation coefficient (right panel).

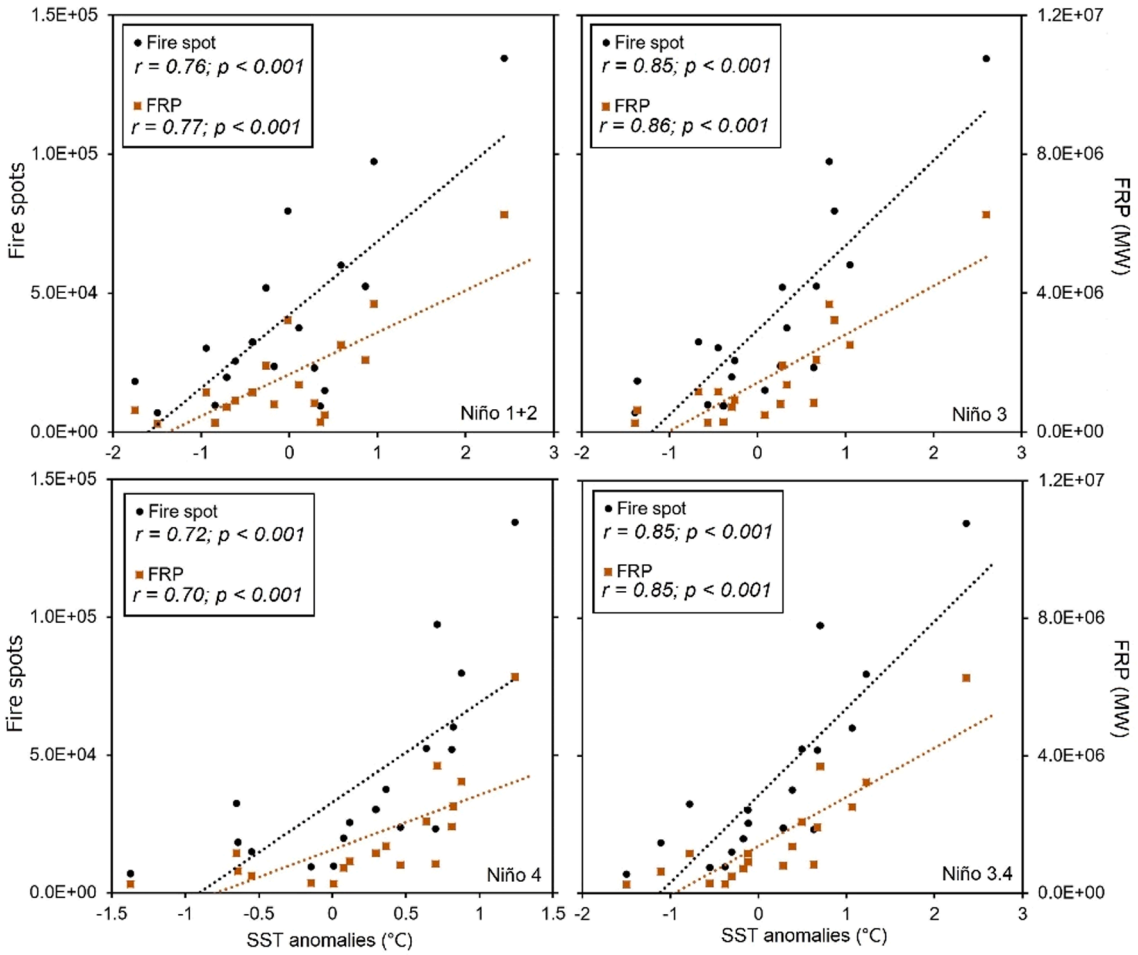

Fig. 8. Correlation between SST anomalies within the four Niño regions and BB in equatorial SEA (second half of the year).

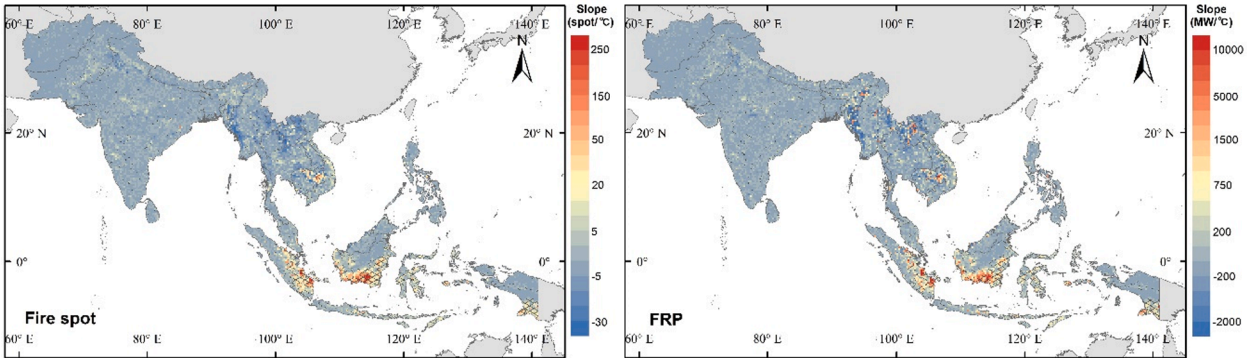

Fig. 9. Correlation between annual SST anomalies in Niño 3 region and annual BB from 2001 to 2018.

and northern Laos was negatively affected by El Niño events. The slopes in these regions reached −50 spots/°C and −10,000 MW/°C, respectively, and they were also insignificant ($p > 0.05$). Fig. 9 reveals that the SST anomalies in the Niño 3 region exhibited hardly any effect on the BB in SA.

3.4.2. *The distribution and variation of average FRP*

Fig. 10 indicated that the average FRP along the India-Myanmar border, in northern Laos, and in eastern Myanmar was much higher than that in the other regions, and the average FRP of certain grids even exceeded 200 MW/spot. As discussed in Section 3.1, the regions were characterized by severe forest fires. The average FRP of forest fires in SA/SEA was 53.1 MW/spot, which was the largest of the BB types, followed by shrubland fires (40.3 MW/spot), other fires (33.0 MW/spot), and CRB (22.2 MW/spot). The dense forests in these regions provided abundant fuel loads; therefore, they were likely to release more radiant energy when a fire occurred. Table 1 and Fig. 10 demonstrate that the average FRP in mainland SEA was higher than that in the other regions, which was likely induced by the local large number and high proportion of forest fires. Because the principal form of BB in SA was CRB, the average FRP in most parts of this region ranged from 25 MW/spot to 30 MW/spot, which was much lower than that in mainland and equatorial SEA. Moreover, the SA annual average FRP presented a significant declining trend which decreased from 43.0 MW/spot in 2001 to only

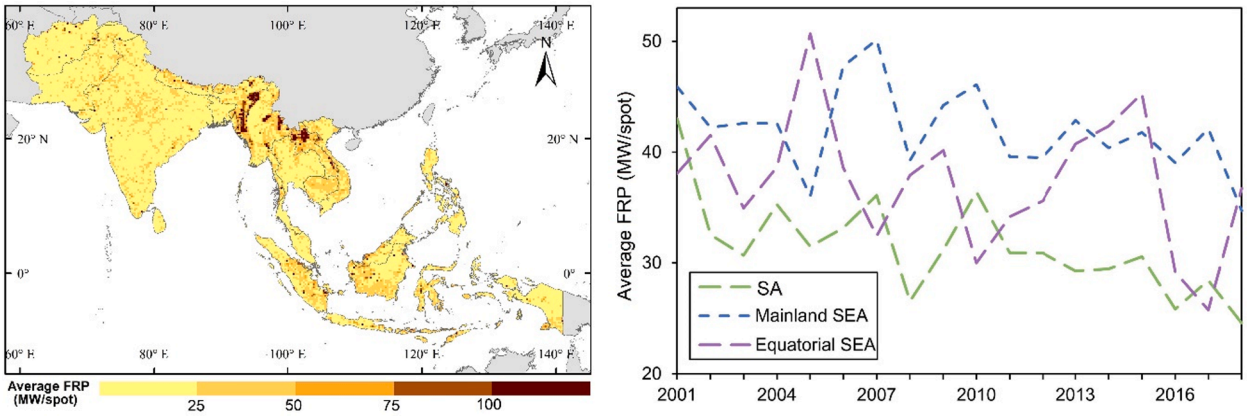

Fig. 10. Spatial distribution of average FRP (left panel) and its interannual variation over SA/SEA (right panel).

25.6 MW/spot in 2018. This was assumed to be primarily due to two reasons. First, CRB, with the lowest average FRP, substantially increased in SA, and the number of fire spots nearly doubled from 2001 to 2018. Second, the intense forest and shrubland fires along the India-Myanmar border significantly declined, and the more scattered burning in this region likely released less energy per spot than that released by the aggregated burning. Similar to the results presented in Fig. 3, the interannual variation in average FRP also severely fluctuated in equatorial SEA, and the value was always larger during El Niño years. In 2005, the average FRP reached 50.7 MW/spot, which was twice as large as the lowest value in 2017. When the severe 2015 Indonesian fire occurred, the average FRP of equatorial SEA was the second largest (45.3 MW/spot).

4. Conclusion

In this study, MODIS active fire and land use products were integrated to classify and evaluate BB spatiotemporal variations over SA/SEA. Because the BB time series in equatorial SEA was too noisy, a more robust trend analysis, Siegel's repeated median, was adopted to reduce the influence of outliers. Additionally, a monotonic trend analysis (MK test) and two geographic distribution analyses (SDE and MEC) were conducted to further quantify the interannual variations and summarize the spatial characteristics of BB. Finally, the influence of rainfall and ENSO were fully explored. The results indicated that BB in SA was dominated by CRB, which accounted for 57.30% of the annual BB spots. From 2001 to 2018, CRB in SA significantly increased by 844 spots/yr, and the MK τ reached 0.61. The increase region was primarily distributed in central/southern India and eastern Pakistan. CRB in Punjab-Haryana, which was characterized by severe CRB and deemed a significant source of air pollution for the Indo-Gangetic Plain, presented a substantial declining trend. This indicates that the measures implemented by local governments effectively mitigate CRB in Punjab-Haryana; however, the increase in CRB in central/southern India and eastern Pakistan still require more attention, which is indispensable in improving the air quality in SA. The number of fire spot and FRP show that BB in mainland SEA was significantly more intense than that in the other regions, and the principal forms are forest and shrubland fires, which accounted for over 70% of the annual spots and over 80% of the annual FRP. Forest fires in mainland SEA declined at a rate of −209 spots/yr, and shrubland fires conversely grew at a rate of 803 spots/yr, which was likely related to the dramatic land cover changes induced by local swidden agriculture. Additionally, forest and shrubland fires along the India-Myanmar border were substantially reduced. Unlike the other regions, BB in equatorial SEA primarily occurred in the second half of the year, and shrubland fires constituted over 50% of the local BB. BB in equatorial SEA was extremely vulnerable to El Niño events, and when the annual SST anomalies within the Niño 3 region improved by 1 °C, the annual number of BB spots and FRP of equatorial SEA increased by 51,800 and 2.40 $\times$ 10^6 MW, respectively. During the strong 2014–2016 El Niño event, the number of BB spots and FRP in equatorial SEA surged to 145,000 and 6.58 $\times$ 10^6 MW, respectively, which were much larger than those in the other years. Although the interannual variation in equatorial SEA is dramatic, the RME still reveals that the BB significantly declined by −1825 spots/yr and that as the principal form of BB, shrubland fires declined by −1083 spots/yr. This decreasing trend reflects the Indonesian government endeavors to curb indigenous BB and restore peatland ecosystems. However, taking substantial measures to reduce anthropogenic fire sources remains imperative in preventing devastating BB during El Niño events.

CRediT authorship contribution statement

Shuai Yin: Conceptualization, Methodology, Software, Visualization, Validation, Writing - original draft, Writing - review & editing.

Declaration of Competing Interest

The authors declare that they have no known competing financial interests or personal relationships that could have appeared to influence the work reported in this paper.

Acknowledgements

We are grateful to NASA, TerraClimate and NOAA for the use of their data. Without their hardworking, we cannot obtain sufficient data to support this study. We also thank the anonymous reviewers whose comments and suggestions helped a lot to improve and clarify this manuscript.

Appendix A. Supplementary material

Supplementary data to this article can be found online at https://doi.org/10.1016/j.envint.2020.106153.

References

Abatzoglou, J.T., Dobrowski, S.Z., Parks, S.A., Hegewisch, K.C., 2018. TerraClimate, a high-resolution global dataset of monthly climate and climatic water balance from 1958–2015. Sci. Data 5, 170191.

Akagi, S.K., Yokelson, R.J., Wiedinmyer, C., Alvarado, M.J., Reid, J.S., Karl, T., Crounse, J.D., Wennberg, P.O., 2011. Emission factors for open and domestic biomass burning for use in atmospheric models. Atmos. Chem. Phys. 11 (9), 4039–4072.

Afroz, R., Hassan, M.N., Ibrahim, N.A., 2003. Review of air pollution and health impacts in Malaysia. Environ. Res. 92 (2), 71–77.

Arbex, M.A., Martins, L.C., de Oliveira, R.C., Pereira, L.A.A., Arbex, F.F., Cançado, J.E.D., Saldiva, P.H.N., Braga, A.L.F., 2007. Air pollution from biomass burning and asthma

hospital admissions in a sugar cane plantation area in Brazil. J. Epidemiol. Community Health 61 (5), 395–400.
Arbex, M.A., Saldiva, P.H.N., Pereira, L.A.A., Braga, A.L.F., 2010. Impact of outdoor biomass air pollution on hypertension hospital admissions. J. Epidemiol. Community Health 64 (7), 573–579.
Auffhammer, M., Ramanathan, V., Vincent, J.R., 2012. Climate change, the monsoon, and rice yield in India. Clim. Change 111 (2), 411–424.
Bhuvaneshwari, S., Hettiarachchi, H., Meegoda, J.N., 2019. Crop residue burning in India: policy challenges and potential solutions. Int. J. Environ. Res. Public Health 16, 832.
Bo, Y., Cai, H., Xie, S.D., 2008. Spatial and temporal variation of historical anthropogenic NMVOCs emission inventories in China. Atmos. Chem. Phys. 8 (23), 7297–7316.
Bond-Lamberty, B., Peckham, S.D., Ahl, D.E., Gower, S.T., 2007. Fire as the dominant driver of central Canadian boreal forest carbon balance. Nature 450, 89–92.
Chang, D., Song, Y., 2010. Estimates of biomass burning emissions in tropical Asia based on satellite-derived data. Atmos. Chem. Phys. 10, 2335–2351.
Engling, G., Zhang, Y.N., Chan, C.Y., Sang, X.F., Lin, M., Ho, K.F., Li, Y.S., Lin, C.Y., Lee, J.J., 2011. Characterization and sources of aerosol particles over the southeastern Tibetan Plateau during the Southeast Asia biomass-burning season. Tellus B Chem. Phys. Meteorol. 63 (1), 117–128.
Fox, J., Castella, J.C., Ziegler, A.D., 2014. Swidden, rubber and carbon: can REDD+ work for people and the environment in montane mainland Southeast Asia? Glob. Environ. Chang. 29, 318–326.
Fox, J., Fujita, Y., Ngidang, D., Peluso, N., Potter, L., Sakuntaladewi, N., Sturgeon, J., Thomas, D., 2009. Policies, political-economy, and swidden in Southeast Asia. Hum. Ecol. 37 (3), 305–322.
Giglio, L., Descloitres, J., Justice, C.O., Kaufman, Y.J., 2003. An enhanced contextual fire detection algorithm for MODIS. Remote Sens. Environ. 87, 273–282.
Giglio, L., Schroeder, W., Justice, C.O., 2016. The collection 6 MODIS active fire detection algorithm and fire products. Remote Sens. Environ. 178, 31–41.
Goldammer, J.G., Seibert, B., 1990. The impact of droughts and forest fires on tropical lowland rain forest of East Kalimantan. Fire in the tropical biota. Springer, Berlin, Heidelberg.
Hamed, K.H., 2009. Exact distribution of the Mann-Kendall trend test statistic for persistent data. J. Hydrol. 365 (1–2), 86–94.
Hao, W.M., Liu, M.H., 1994. Spatial and temporal distribution of tropical biomass burning. Glob. Biogeochem Cycles 8 (4), 495–503.
Hayasaka, H., Noguchi, I., Putra, E.I., Yulianti, N., Vadrevu, K., 2014. Peat-fire-related air pollution in Central Kalimantan, Indonesia. Environ. Pollut. 195, 257–266.
Itahashi, S., Uno, I., Irie, H., Kurokawa, J.I., Ohara, T., 2018. Impacts of biomass burning emissions on tropospheric NO2 vertical column density over continental Southeast Asia. In: Land-Atmospheric Research Applications in South and Southeast Asia. Springer, Cham.
Jethva, H., Torres, O., Field, R.D., Lyapustin, A., Gautam, R., Kayetha, V., 2019. Connecting crop productivity, residue fires, and air quality over northern India. Sci. Rep. 9 (1), 1–11.
Justice, C.O., Giglio, L., Korontzi, S., Owens, J., Morisette, J.T., Roy, D., Descloitres, J., Alleaume, S., Petitcolin, F., Kaufman, Y., 2002. The MODIS fire products. Remote Sens. Environ. 83, 244–262.
Kanapathy, K., 1976. Fertilizer requirement on peat soils. Malays. Agri. J. 50, 292–307.
Kaskaoutis, D.G., Kumar, S., Sharma, D., Singh, R.P., Kharol, S.K., Sharma, M., Singh, A. K., Singh, S., Singh, A., Singh, D., 2014. Effects of crop residue burning on aerosol properties, plume characteristics, and long-range transport over northern India. J. Geophys. Res. Atmos. 119 (9), 5424–5444.
Kendall, M.G., 1955. Rank Correlation Methods Griffin, London.
Koe, L.C., Arellano Jr, A.F., McGregor, J.L., 2001. Investigating the haze transport from 1997 biomass burning in Southeast Asia: its impact upon Singapore. Atmos. Environ. 35 (15), 2723–2734.
Konovalov, I.B., Berezin, E.V., Ciais, P., Broquet, G., Beekmann, M., Hadji-Lazaro, J., Clerbaux, C., Andreae, M.O., Kaiser, J.W., Schulze, E.D., 2014. Constraining CO_2 emissions from open biomass burning by satellite observations of co-emitted species: a method and its application to wildfires in Siberia. Atmos. Chem. Phys. 14, 10383–10410.
Kumar, R., Naja, M., Satheesh, S.K., Ojha, N., Joshi, H., Sarangi, T., Pant, P., Dumka, U. C., Hegde, P., Venkataramani, S., 2011. Influences of the springtime northern Indian biomass burning over the central Himalayas. J. Geophys. Res. Atmos. 116 (D19).
Lavagnini, I., Badocco, D., Pastore, P., Magno, F., 2011. Theil-Sen nonparametric regression technique on univariate calibration, inverse regression and detection limits. Talanta 87, 180–188.
Lawrence, M.G., Rasch, P.J., von Kuhlmann, R., Williams, J., Fischer, H., de Reus, M., Lelieveld, J., Crutzen, P.J., Schultz, M., Stier, P., Huntrieser, H., Heland, J., Stohl, A., Forster, C., Elbern, H., Jakobs, H., Dickerson, R.R., 2003. Global chemical weather forecasts for field campaign planning: predictions and observations of large-scale features during MINOS, CONTRACE, and INDOEX. Atmos. Chem. Phys. 3, 267–289.
Lefever, D.W., 1926. Measuring geographic concentration by means of the standard deviational ellipse. Am. J. Sociol. 32 (1), 88–94.
Lelieveld, J.O., Crutzen, P.J., Ramanathan, V., Andreae, M.O., Brenninkmeijer, C.A.M., Campos, T., Cass, G.R., Dickerson, R.R., Fischer, H., De Gouw, J.A., Hansel, A., 2001. The Indian Ocean experiment: widespread air pollution from South and Southeast Asia. Science 291 (5506), 1031–1036.
Lemmens, S., Krag, H., 2014. Two-line-elements-based maneuver detection methods for satellites in low earth orbit. J. Guid. Control Dynam 37 (3), 860–868.
Lin, H., Wang, X., Qian, Z.M., Guo, S., Yao, Z., Vaughn, M.G., Dong, G., Liu, T., Xiao, J., Li, X., Zeng, W., 2018. Daily exceedance concentration hours: a novel indicator to measure acute cardiovascular effects of $PM_{2.5}$ in six Chinese subtropical cities. Environ. Int. 111, 117–123.
Lin, Y.-H., Zhang, H., Pye, H.O., Zhang, Z., Marth, W.J., Park, S., Arashiro, M., Cui, T., Budisulistiorini, S.H., Sexton, K.G., Vizuete, W., Xie, Y., Luecken, D.J., Piletic, I.R., Edney, E.O., Bartolotti, L.J., Gold, A., Surratt, J.D., 2013. Epoxide as a precursor to secondary organic aerosol formation from isoprene photooxidation in the presence of nitrogen oxides. Proc. Natl. Acad. Sci. U.S.A. 110, 6718–6723.
Liu, H., Chang, W.L., Oltmans, S.J., Chan, L.Y., Harris, J.M., 1999. On springtime high ozone events in the lower troposphere from Southeast Asian biomass burning. Atmos. Environ. 33 (15), 2403–2410.
Lorenz, K., Lal, R., 2010. Carbon Sequestration in Forest Ecosystems. Springer, the Netherlands.
Loveland, T.R., Belward, A.S., 1997. The IGBP-DIS global 1km land cover data set, DISCover: first results. Int. J. Remote Sens. 18 (15), 3289–3295.
Mann, H.B., 1945. Nonparametric tests against trend. Econometrica 13, 245–259.
Marlier, M.E., DeFries, R.S., Voulgarakis, A., Kinney, P.L., Randerson, J.T., Shindell, D.T., Chen, Y., Faluvegi, G., 2013. El Niño and health risks from landscape fire emissions in southeast Asia. Nat. Clim. Change 3 (2), 131.
McClure, C.D., Jaffe, D.A., 2018. Investigation of high ozone events due to wildfire smoke in an urban area. Atmos. Environ. 194, 146–157.
Mertz, O., Padoch, C., Fox, J., Cramb, R.A., Leisz, S.J., Lam, N.T., Vien, T.D., 2009. Swidden change in Southeast Asia: understanding causes and consequences. Hum. Ecol. 37 (3), 259–264.
Miettinen, J., Shi, C., Liew, S.C., 2016. 2015 Land cover map of Southeast Asia at 250 m spatial resolution. Remote Sens. Lett. 7, 701–710.
Myhre, G., Samset, B.H., Schulz, M., Balkanski, Y., Bauer, S., Berntsen, T.K., Bian, H., Bellouin, N., Chin, M., Diehl, T., Easter, R.C., Feichter, J., Ghan, S.J.,Hauglustaine, D., Iversen, T., Kinne, S., Kirkevåg, A., Lamarque, J.-F., Lin, G., Liu, X., Lund, M.T., Luo, G., Ma, X., van Noije, T., Penner, J.E., Rasch, P.J., Ruiz, A.,Seland, ø, Skeie, R. B., Stier, P., Takemura, T., Tsigaridis, K., Wang, P., Wang, Z.,Xu, L., Yu, H., Yu, F., Yoon, J.-H., Zhang, K., Zhang, H., Zhou, C., 2013. Radiative forcing of the direct aerosol effect from AeroCom Phase II simulations. Atmos. Chem. Phys. 13(4), 1853–1877.
Park, M., Randel, W.J., Gettelman, A., Massie, S.T., Jiang, J.H., 2007. Transport above the Asian summer monsoon anticyclone inferred from Aura Microwave Limb Sounder tracers. J. Geophys. Res. 112, D16309.
Pun, V.C., Kazemiparkouhi, F., Manjourides, J., Suh, H.H., 2017. Long-term $PM_{2.5}$ exposure and respiratory, cancer, and cardiovascular mortality in older US adults. Am. J. Epidemiol. 186 (8), 961–969.
Reddington, C.L., Butt, E.W., Ridley, D.A., Artaxo, P., Morgan, W.T., Coe, H., Spracklen, D.V., 2015. Air quality and human health improvements from reductions in deforestation-related fire in Brazil. Nat. Geosci. 8 (10), 768.
Rerkasem, K., Lawrence, D., Padoch, C., Schmidt-Vogt, D., Ziegler, A.D., Bruun, T.B., 2009. Consequences of swidden transitions for crop and fallow biodiversity in Southeast Asia. Hum. Ecol. 37 (3), 347–360.
Sahu, L.K., Sheel, V., 2014. Spatio-temporal variation of biomass burning sources over South and Southeast Asia. J. Atmos. Chem. 71 (1), 1–19.
Sen, P.K., 1968. Estimates of the regression coefficient based on Kendall's tau. J. Am. Stat. Assoc. 63, 1379–1389.
Sharma, A.R., Kharol, S.K., Badarinath, K.V.S., Singh, D., 2010. Impact of agriculture crop residue burning on atmospheric aerosol loading-a study over Punjab State, India. Ann. Geophys. 28 (2).
Shi, Y., Sasai, T., Yamaguchi, Y., 2014. Spatio-temporal evaluation of carbon emissions from biomass burning in Southeast Asia during the period 2001–2010. Ecol. Model. 272, 98–115.
Siegel, A.F., 1982. Robust regression using repeated medians. Biometrika 69 (1), 242–244.
Stibig, H.-J., Achard, F., Carboni, S., Raši, R., Miettinen, J., 2014. Change in Tropical Forest Cover of Southeast Asia from 1990 to 2010. Biogeosciences 11, 247–258.
Theil, H., 1950. A rank invariant method of linear and polynomial regression analysis, part 3. Proceedings of Koninalijke Nederlandse Akademie van Weinenschatpen A 53, 1397–1412.
Turetsky, M.R., Benscoter, B., Page, S., Rein, G., van der Werf, G.R., Watts, A., 2015. Global vulnerability of peatlands to fire and carbon loss. Nat. Geosci. 8 (1), 11–14.
van der Werf, G.R., Randerson, J.T., Giglio, L., Collatz, G.J., Mu, M., Kasibhatla, P.S., Morton, D.C., DeFries, R.S., Jin, Y.V., van Leeuwen, T.T., 2010. Global fire emissions and the contribution of deforestation, savanna, forest, agricultural, and peat fires (1997–2009). Atmos. Chem. Phys. 10 (23), 11707–11735.
Vanem, E., Walker, S.E., 2013. Identifying trends in the ocean wave climate by time series analyses of significant wave heightdata. Ocean Eng. 61, 148–160.
Wang, B., Shi, W., Miao, Z., 2015. Confidence analysis of standard deviational ellipse and its extension into higher dimensional Euclidean space. PloS one 10 (3), e0118537.
Xiong, X., Che, N., Barnes, W.L., 2006. Terra MODIS on-orbit spectral characterization and performance. IEEE Trans. Geosci. Remote Sens. 44 (8), 2198–2206.
Xiong, X., Wu, A., Wenny, B.N., Madhavan, S., Wang, Z., Li, Y., Chen, N., Barnes, W.L., Salomonson, V.V., 2015. Terra and Aqua MODIS thermal emissive bands on-orbit calibration and performance. IEEE Trans. Geosci. Remote Sens. 53 (10), 5709–5721.
Yin, S., Wang, X., Zhang, X., Guo, M., Miura, M., Xiao, Y., 2019. Influence of biomass burning on local air pollution in mainland Southeast Asia from 2001 to 2016. Environ. Pollut. 254, 112949.